Electronic Supplementary Information

Seeded-growth Synthesis of Dispersed Co_9S_8 Nanoparticles Loaded in Carbon Aerogel as Efficient Bi-catalysts towards ORR and HER

Hetong Fang, [a,b] Hang Lv, [a] Xuehui Liu,[a] Shengnan Li [a] and Haibing Xia [*a]

[a] State Key Laboratory of Crystal Materials, Shandong University, Jinan, 250100, P. R. China;

[b] SDU-ANU Joint Science College, Shandong University at Weihai, Weihai 264209, P. R. China

1. Experimental section

1.1 *Materials:*

Iron (III) nitrate nonahydrate ($Fe(NO_3)_3 \cdot 9H_2O$, 98.5+%), Tannic acid ($C_{76}H_{52}O_{46}$, 98+%), hydrochloric acid (HCl, CAS number: 7647-01-0, 36.46%), and ammonium persulfate (APS, 98+%) were purchased from National Reagent Company. Cobalt nitrate hexahydrate ($Co(NO_3)_2 \cdot 6H_2O$, 98.00%) was purchased from Aladdin (Shanghai, China). Aniline hydrochloride ($C_6H_5NH_2 \cdot HCl$, 99.00%) was purchased from Alfa Aesar (Shanghai, China). All chemical reagents were used without further purification. All glass wares were washed with aqua regia and then rinsed thoroughly with ultrapure water and dried before use.

1.2 *Materials characterizations:*

Low-resolution transmission electron microscopy (TEM) and high-resolution TEM (HRTEM) images were obtained by a JEOL JEM-2100F transmission electron microscope with an accelerating voltage of 200 kV. High-angle annular dark field-scanning TEM (HAADF-STEM) images were investigated by a FEI Titan G2 80-200 ChemiSTEM electron microscope with an accelerating voltage of 200 kV. The X-ray diffraction (XRD) analysis was carried out on a Bruker AXSD8 advance X-ray diffractometer equipped with Cu Kα radiation with a scanning angle (2θ) of 20−90° range with a step size of 0.04°. Raman spectra were collected with a RAM II Raman spectrometer from Broker at the excitation of a 633 nm laser. X-ray photoelectron spectra (XPS) was obtained on an ESCALAB 250 spectrometer with a monochromatic Al anode (Al Kα=1.4866 keV).

1.3 *Electrochemical measurements of HER and ORR:*

All electrochemical tests were carried out in a three-electrode on CHI 601E electrochemical workstation at room temperature.

The HER polarization curves were acquired in 0.5 M H_2SO_4 solution, with the Ag/AgCl electrode as the reference electrode, a graphite electrode as the counter electrode, and a 3.0 mm glassy carbon electrode with catalysts as the working electrode. To prepare the working electrode, 10 mg of catalysts was firstly dispersed in a mixed solution of 950 μL water and 50 μL of 5 wt% Nafion solution. After sonication for 30 min, a homogeneous ink was formed. Then, 8 μL of ink was deposited onto the working electrode, which was dried in the atmosphere and at room temperature. For comparison, commercial Pt/C catalysts were also prepared as the working electrode with a loading of 25 μg cm^{-2}.

All polarization curves were iR-corrected. Electrochemical impedance spectra (EIS) experiments were tested at the overpotential of each catalyst. The measured potentials versus the Ag/AgCl electrode were normalized to a reversible hydrogen electrode (RHE) scale by the Nernst equation ($E_{RHE} = E_{Ag/AgCl} + 0.0592pH + 0.21$).

The stability of the catalysts was evaluated by 10000 continuous cycles from -0.8 to 0 V (vs. RHE) in 0.5 M H_2SO_4 at a scan rate of 100 mV s^{-1}, and the chronopotentiometry method at the overpotential for 28000 s in 0.5 M H_2SO_4.

The ORR polarization curves were acquired in 0.1 M KOH electrolyte, with 5.0 mm glassy carbon rotating disk electrode as the working electrode, a double salt bridge saturated calomel electrode as a reference electrode which was immersed in saturated potassium chloride for more than one day before using, and a platinum wire as a counter electrode separated from the solution by an ion exchange membrane, respectively. The measured potentials versus Hg/Hg_2Cl_2 were normalized to a reversible hydrogen electrode (RHE) scale by the Nernst equation ($E_{RHE} = E_{Hg/Hg_2Cl_2} + 0.0592pH + 0.242$). The homogenous catalysts ink was obtained by mixing the catalysts powder (10 mg) with 950 μL of water and 50 μL of Nafion solution (5 wt%) under sonication for 30 min. Then, 20 μL of ink was dropped onto the glassy carbon (GC) rotating disk electrode, followed by drying at room temperature. For comparison, commercial Pt/C catalysts as a reference were prepared as the working electrode with a loading of 0.2 mg cm^{-2}.

O_2 was bubbled into the cell for at least 30 min prior to each set of experiments, and continuously bubbling during the tests. The scanning rate of CV was 10 mV s^{-1}. The Linear sweep voltammetry (LSV) curves measured at speeds of 400, 625, 900, 1225, and 1600 rpm with a scan rate of 5.0 mV s^{-1}. Solution ohmic drop (i.e., iR drop) was compensated. The electron transfer number during the ORR process was determined by the Koutecky-Levich equation:

$$\frac{1}{j} = \frac{1}{j_L} + \frac{1}{j_k} = \frac{1}{B\omega^{\frac{1}{2}}} + \frac{1}{j_k}$$

$$B = 0.62nFC_0D_0^{2/3}v^{-1/6}$$

where j represents the measured current density, j_k and j_L are the kinetic current density and the diffusion limiting current density. ω is the angular velocity applied in the test, F is Faraday constant (96485 C mol^{-1}), the bulk concentration of O_2 in electrolyte (C_0) is 1.26×10^{-3} mol cm^{-3}, D_0 is the diffusion coefficient of oxygen in 0.1 M KOH (1.9×10^{-5} cm^2 s^{-1}), and the kinetic viscosity is 1.009×10^{-2} cm^2 s^{-1}. Accelerated durability test (ADT) of as-prepared Co_9S_8 $^{7.5}$NP/CA catalysts and commercial Pt/C catalysts were performed in the 0.1 M KOH electrolyte by

applying potential cycling between 0.4 and 0.8 V vs. RHE at a sweep rate of 100 mV s^{-1} for 20000 cycles. The methanol tolerance tests of the as-prepared Co_9S_8 $^{7.5}$NP/CA catalysts and commercial Pt/C catalysts were evaluated by chronoamperometric measurement at 0.8 V (vs. RHE) with an addition of 1 M methanol.

Figure S1. LSV curves of a series of Co/S-based catalysts prepared under different molar ratios of Fe^{3+}-to-Co^{2+} ion.

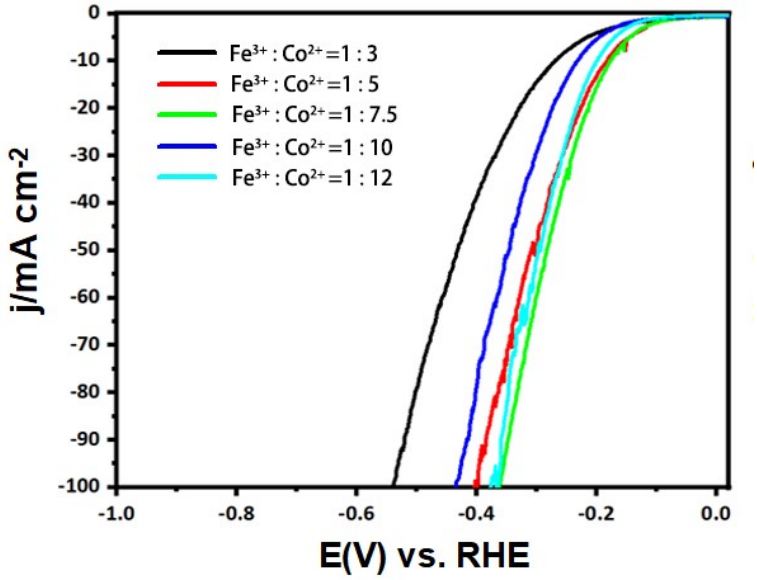

Figure S2. LSV curves of a series of Co/S-based catalysts prepared under different molar ratios of Fe^{3+}-to-TA.

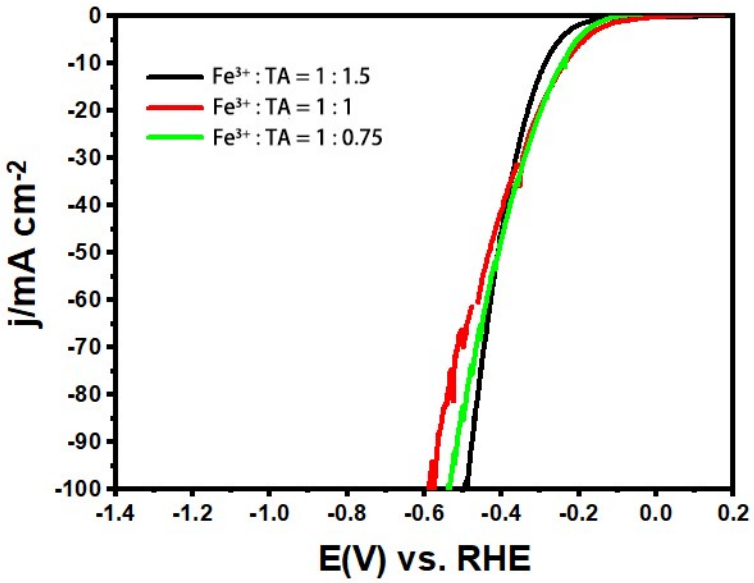

Figure S3. LSV curves of a series of Co/S-based catalysts prepared under different pyrolysis temperatures.

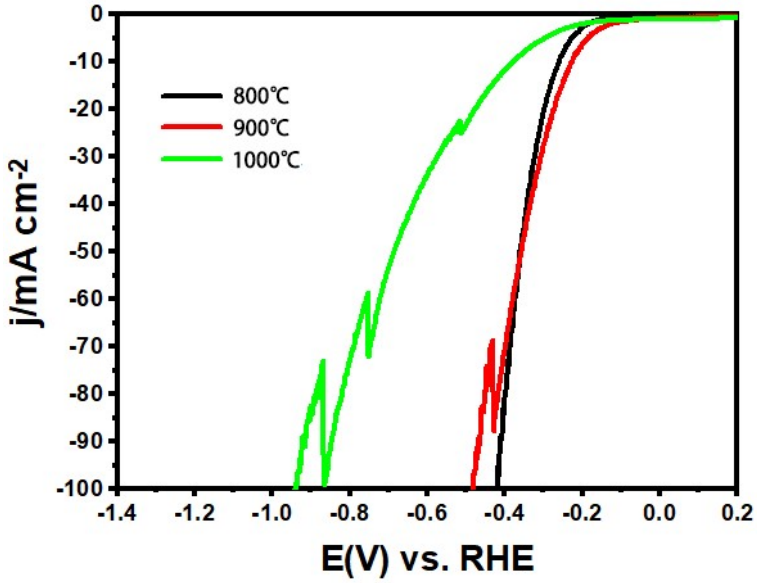

Figure S4. LSV curves of a series of Co/S-based catalysts prepared under different holding time at 900 °C pyrolysis.

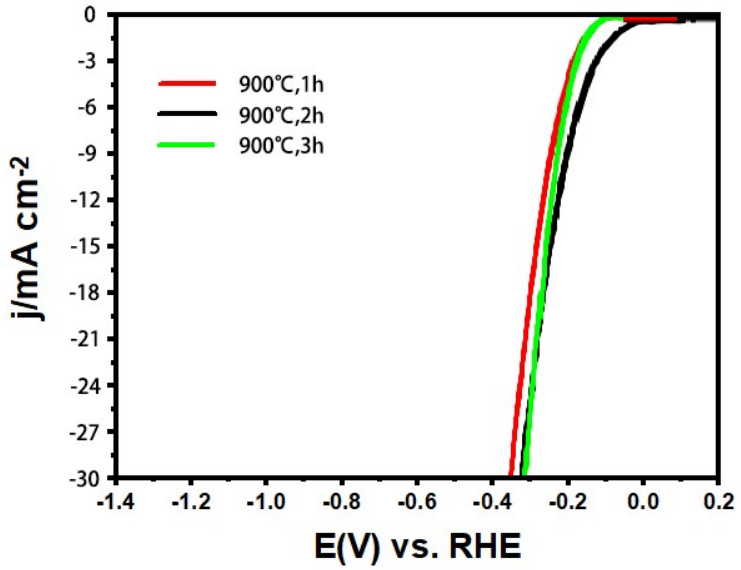

Figure S5. LSV curves of the as-prepared Co_9S_8 $^{7.5}$NP/CA catalysts obtained after the acid-leaching treatments, which were treated by different concentrations of H_2SO_4.

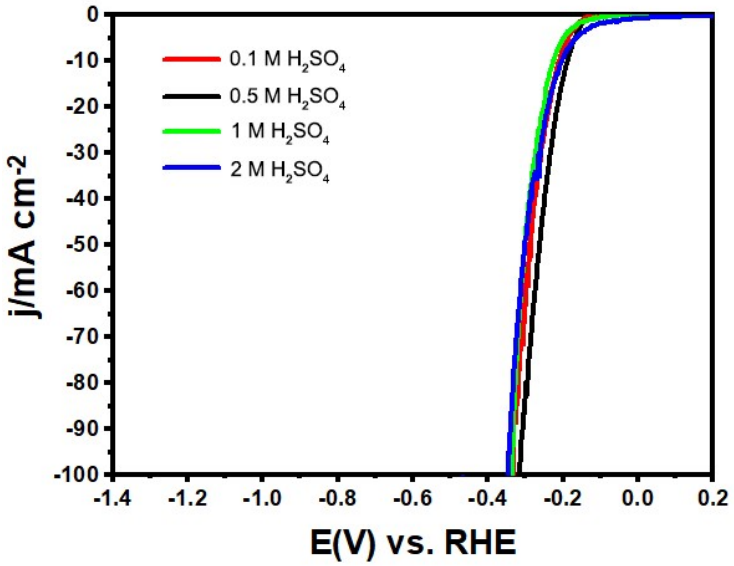

Figure S6. LSV curves of the as-prepared Co_9S_8 $^{7.5}$NP/CA catalysts obtained after the acid-leaching treatments, which were treated by different treatment times at a fixed H_2SO_4 concentration (0.5M).

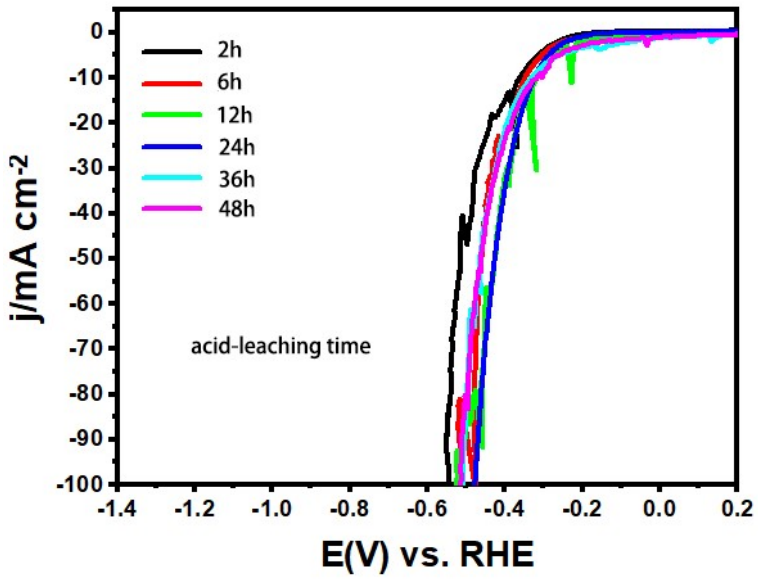

Figure S7. TEM image of polyaniline hydrogels.

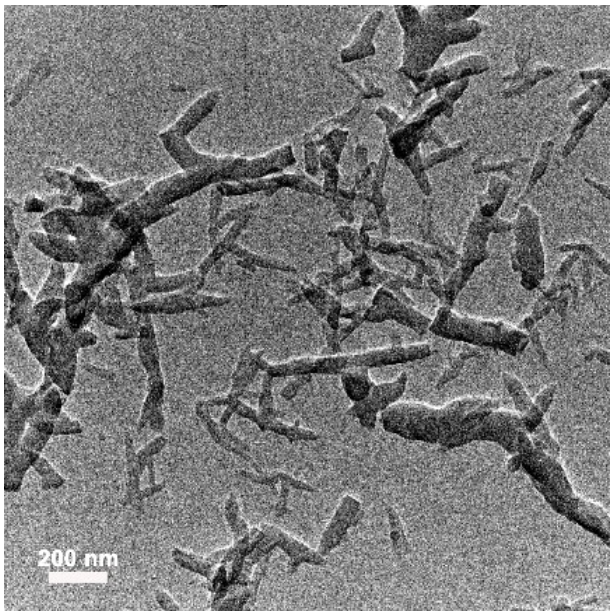

Figure S8. TEM images of (a) Co_9S_8 ^{3}NP/CA catalysts, (b) Co_9S_8 ^{5}NP/CA catalysts, and (c) Co_4S_3 ^{10}NP/CA catalysts.

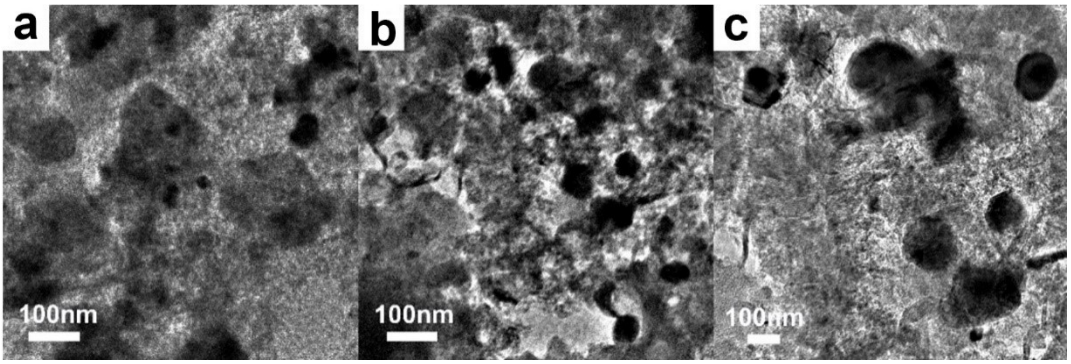

Figure S9. XRD patterns of (a) Co_9S_8 ^{3}NP/CA catalysts, (b) Co_9S_8 ^{5}NP/CA catalysts (c) the as-prepared Co_9S_8 $^{7.5}$NP/CA catalysts, and (d) Co_4S_3 ^{10}NP/CA catalysts.

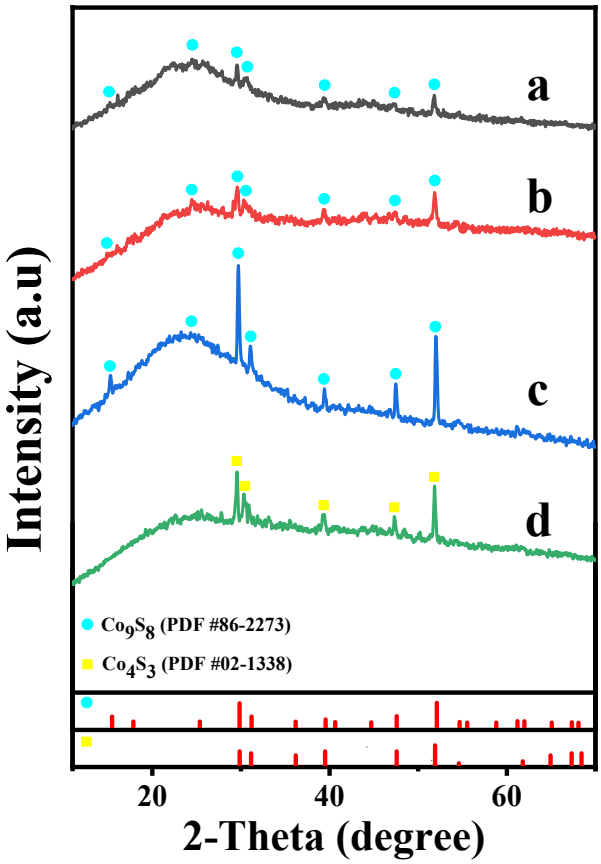

X-ray diffraction (XRD) patterns of Co_9S_8 ^{3}NP/CA catalysts, Co_9S_8 ^{5}NP/CA catalysts, and Co_4S_3 ^{10}NP/CA catalysts was also conducted, which were compared with that of the as-prepared Co_9S_8 $^{7.5}$NP/CA catalysts. All of them exhibit two diffraction peaks at about 25° and 43.8°, which are attributed to (002) and (101) planes of the graphitic carbon, respectively.[1] Moreover, seven diffraction peaks located about 15.4°, 25.4°, 29.8°, 31.2°, 39.5°, 44.7°, and 52.1° are also observed in the Co_9S_8 ^{5}NP/CA catalysts, and Co_9S_8 ^{3}NP/CA catalysts, which are attributed to the (111), (220), (311), (222), (331), (422), and (440) planes of Co_9S_8 (PDF: 86-2273), respectively.[2] The results indicate that active species among Co_9S_8 ^{3}NP/CA catalysts, Co_9S_8 ^{5}NP/CA catalysts and the as-prepared Co_9S_8 $^{7.5}$NP/CA catalysts are all Co_9S_8 NPs. In contrast, five diffraction peaks located about 29.9°, 31.1°, 39.5°, 47.5°, and 51.9° are observed in the Co_4S_3 ^{10}NP/CA catalysts, which are attributed to the (311), (222), (331), (511), and (440) planes of Co_4S_3 (PDF: 02-1338), respectively.[3] The results indicate that when the molar of Co^{2+}-to-Fe^{3+} ion was increased to 10, the active species have indeed become Co_4S_3 ^{10}NPs in the Co_4S_3 ^{10}NP/CA catalysts.

Figure S10. LSV curves of (a) Co_9S_8 ^{3}NP/CA catalysts, (b) Co_9S_8 ^{5}NP/CA catalysts, (c) the as-prepared Co_9S_8 $^{7.5}$NP/CA catalysts, (d) Co_4S_3 ^{10}NP/CA catalysts and (e) CA catalysts which were measured in O_2-saturated 0.1 M KOH solution.

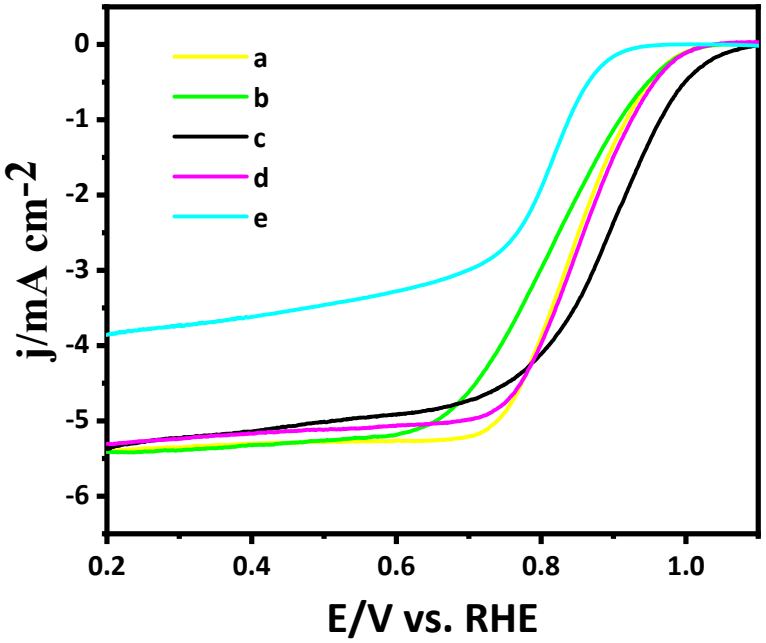

One can clearly see that the half-wave potential ($E_{1/2}$) of the as-prepared Co_9S_8 $^{7.5}$NP/CA catalysts is 0.891 V, which is better than that of Co_9S_8 ^{3}NP/CA catalysts (0.837 V), Co_9S_8 ^{5}NP/CA catalysts (0.846 V), Co_4S_3 ^{10}NP/CA catalysts (0.855 V) and CA catalysts (0.823 V).

Figure S11. LSV curves of (a) Co_9S_8 ^{3}NP/CA catalysts, (b) Co_9S_8 ^{5}NP/CA catalysts, (c) the as-prepared Co_9S_8 $^{7.5}$NP/CA catalysts, (d) Co_4S_3 ^{10}NP/CA catalysts and (e) CA catalysts, which were measured in N_2-saturated 0.5 M H_2SO_4 solution.

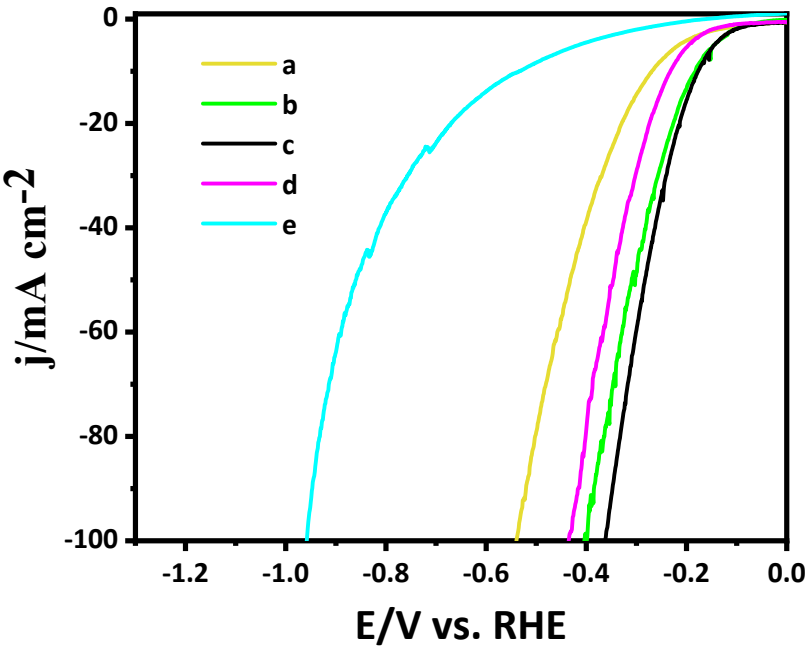

One can clearly see that the overpotential at 10 mA cm^{-2} (η_{10}) of the as-prepared Co_9S_8 $^{7.5}$NP/CA catalysts is about 177 mV, which is smaller than that of Co_9S_8 ^{3}NP/CA catalysts (269 mV), Co_9S_8 ^{5}NP/CA catalysts (182 mV), Co_4S_3 ^{10}NP/CA catalysts (233 mV) and CA catalysts (534 mV).

Figure S12. TEM image of CA catalysts.

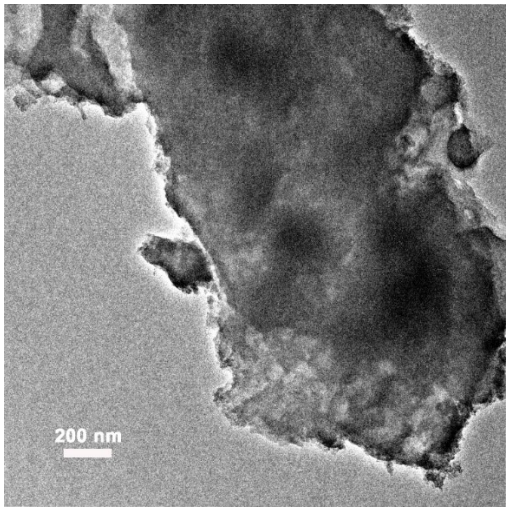

Figure S13. TEM image of pure Co_9S_8 NP/CA catalysts.

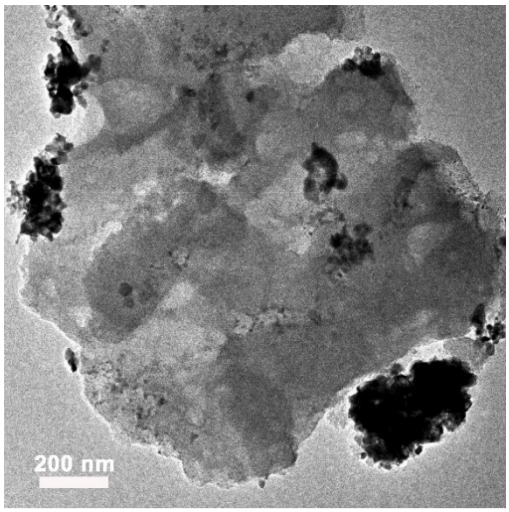

Figure S14. HAADF-STEM image and the corresponding HAADF-STEM-EDS images of the as-prepared Co_9S_8 $^{7.5}$NP/CA catalysts.

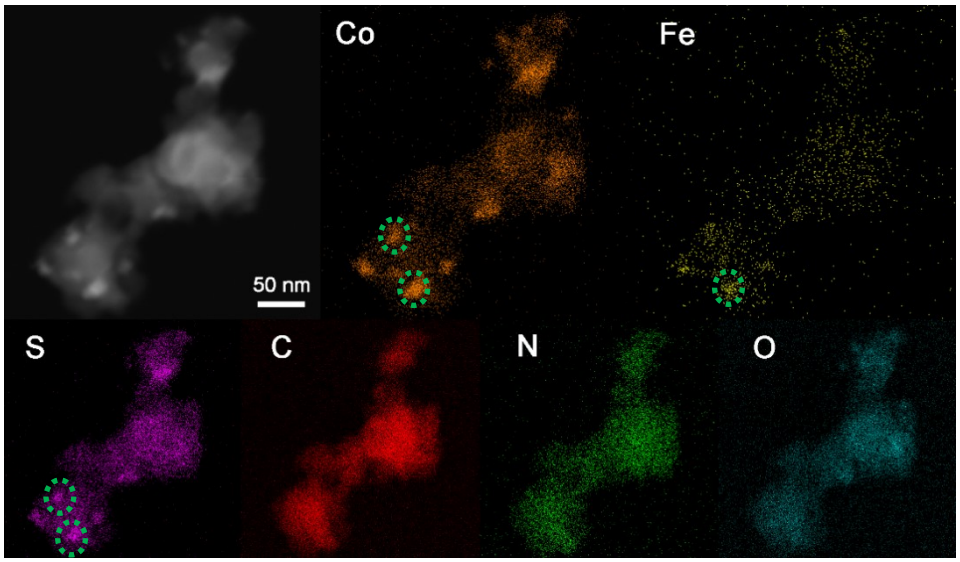

Figure S15. XRD pattern of CA catalysts.

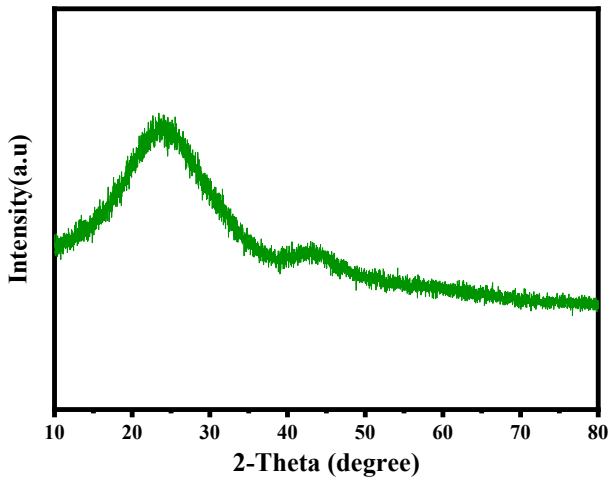

Figure S16. Raman spectrum of CA catalysts.

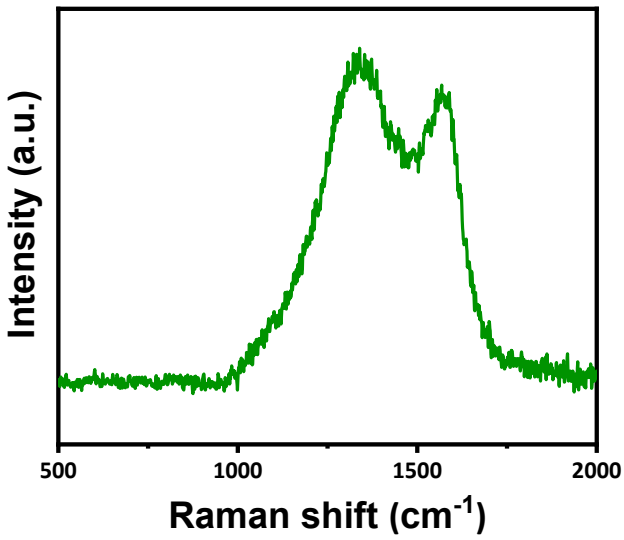

The intensity ratio (ID / IG) of CA catalysts is 1.88.

Figure S17. XPS survey spectrum of pure Co_9S_8 NP/CA catalysts.

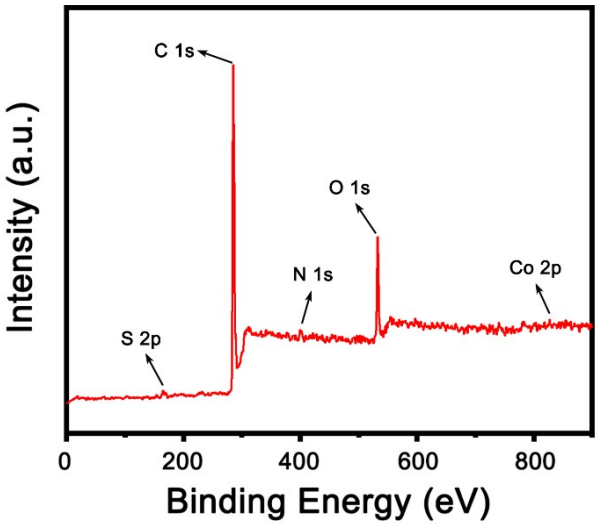

Figure S18. XPS spectrum of Fe 2p of elemental Fe in the as-prepared Co_9S_8 $^{7.5}$NP/CA catalysts.

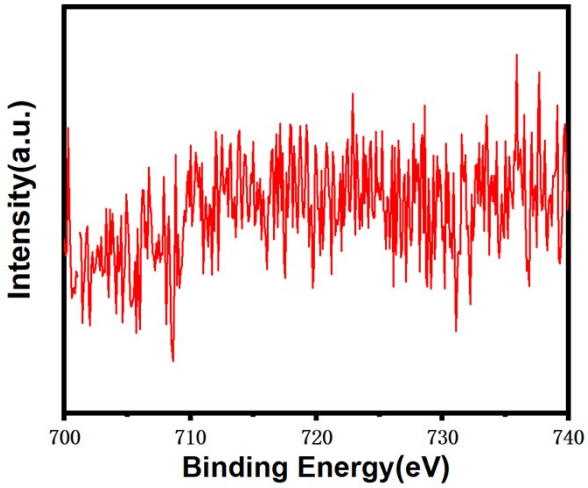

Figure S19. XPS spectra of C 1s of elemental C in the as-prepared Co_9S_8 $^{7.5}$NP/CA catalysts (a) and pure Co_9S_8 NP/CA catalysts (b).

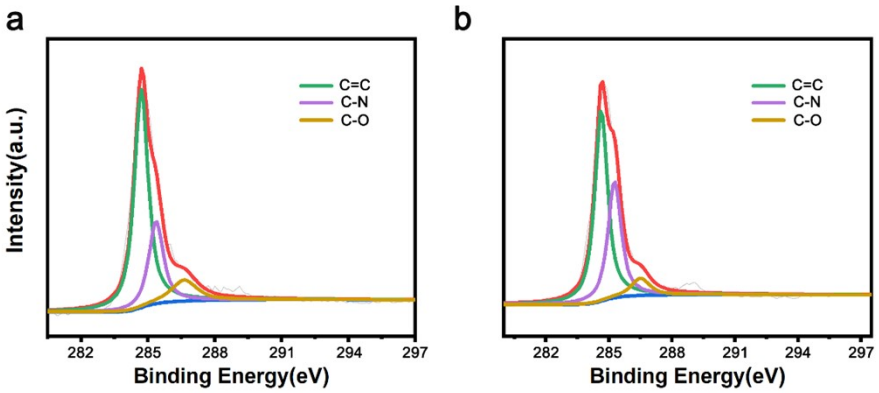

Figure S20. XPS spectra of N 1s of elemental N in the as-prepared Co_9S_8 $^{7.5}$NP/CA catalysts (a) and pure Co_9S_8 NP/CA catalysts (b).

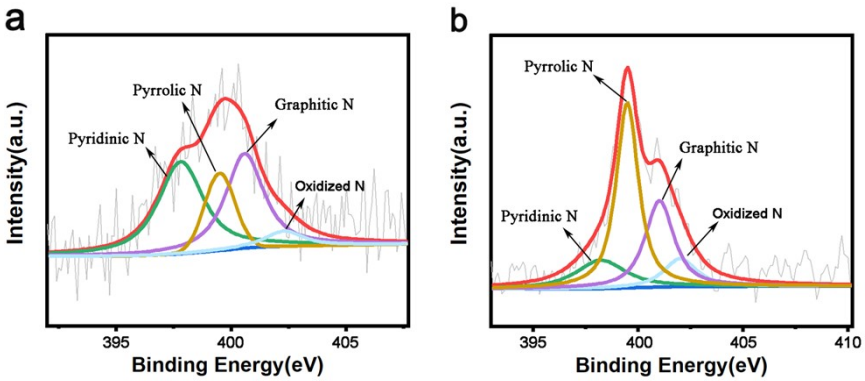

Figure S21. XPS spectra of O 1s of elemental O in the as-prepared Co_9S_8 $^{7.5}$NP/CA catalysts (a) and pure Co_9S_8 NP/CA catalysts (b).

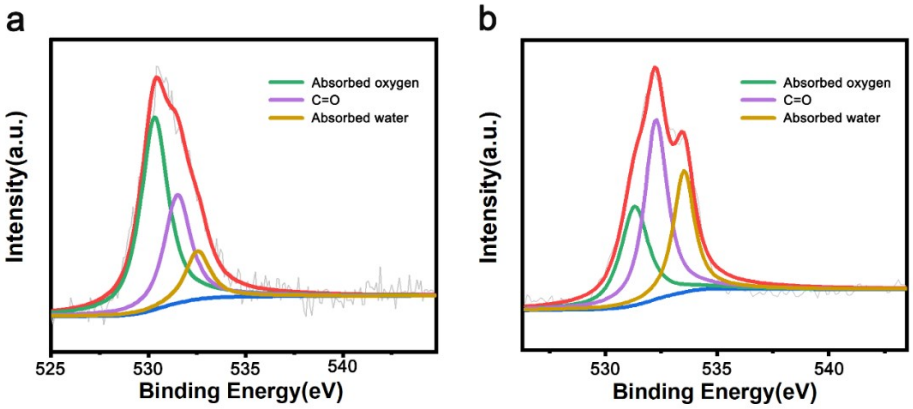

Figure S22. XPS spectrum of S 2p of elemental S in pure Co_9S_8 NP/CA catalysts.

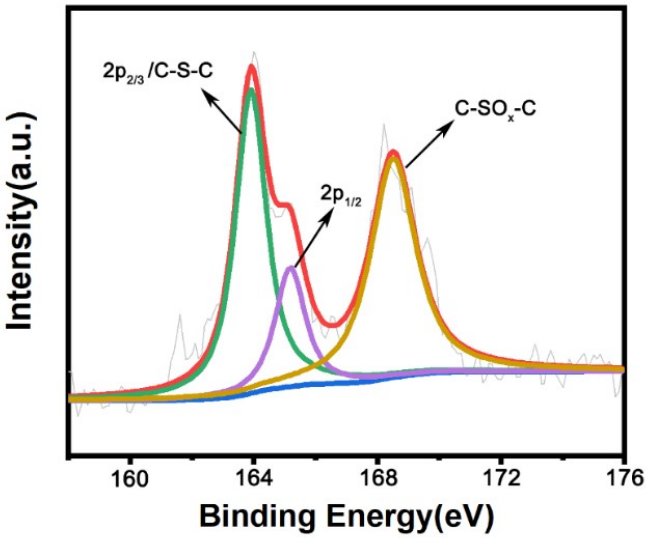

Figure S23. XPS spectrum of Co 2p of elemental Co in pure Co_9S_8 NP/CA catalysts.

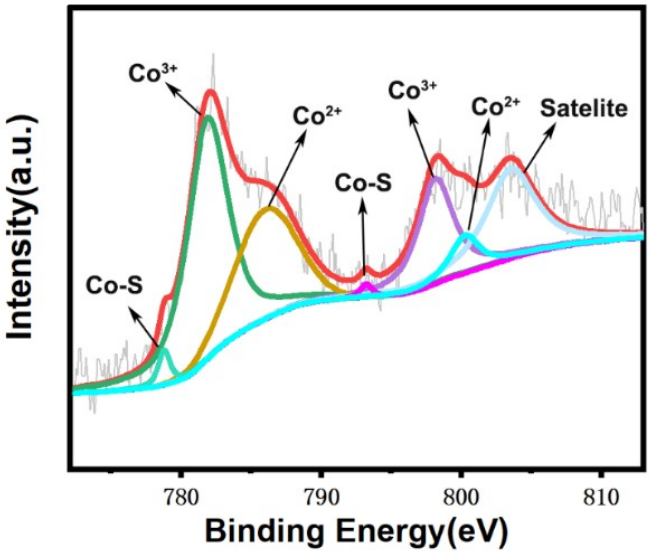

Figure S24. CV curves of (a) commercial Pt/C catalysts and (b) the as-prepared Co_9S_8 $^{7.5}$NP/CA catalysts towards the ORR measured in O_2-saturated 0.1 M KOH solution with a scan rate of 50 mV s^{-1}.

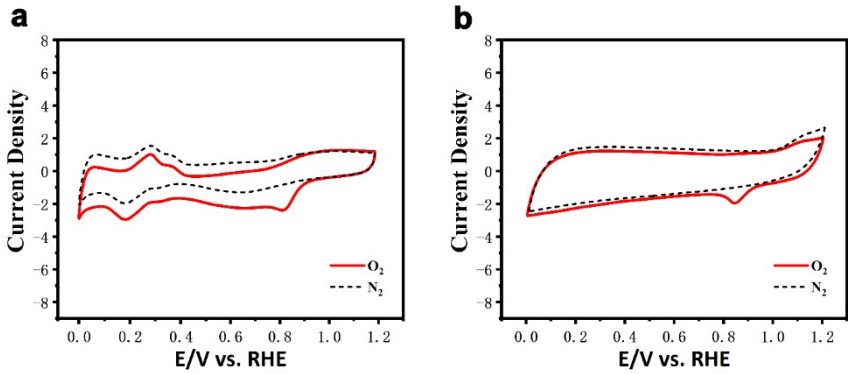

Figure S25. LSV curves of (a) the as-prepared Co_9S_8 $^{7.5}$NP/CA catalysts, (b) pure Co_9S_8 NP/CA catalysts and (c) commercial Pt/C catalysts, which were measured at different rotational speeds ranging from 400 to 1600 rpm.

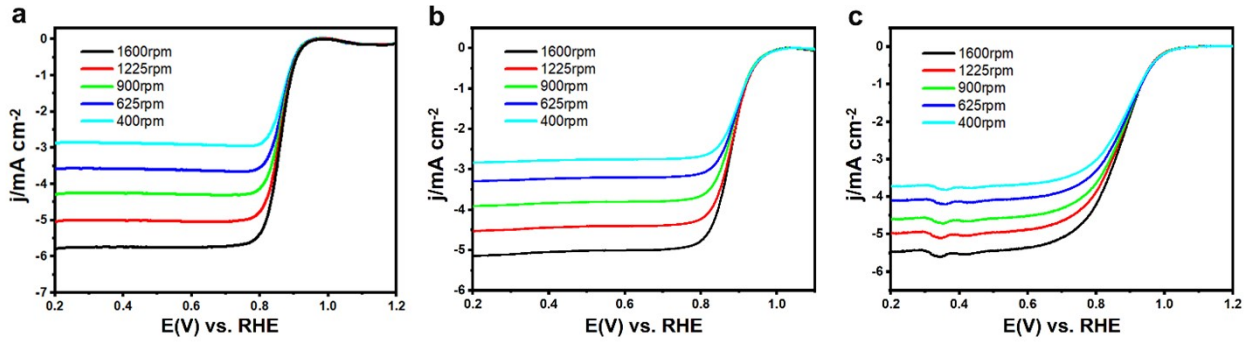

Figure S26. LSV curves of commercial Pt/C catalysts towards the alkaline ORR before and after the ADTs.

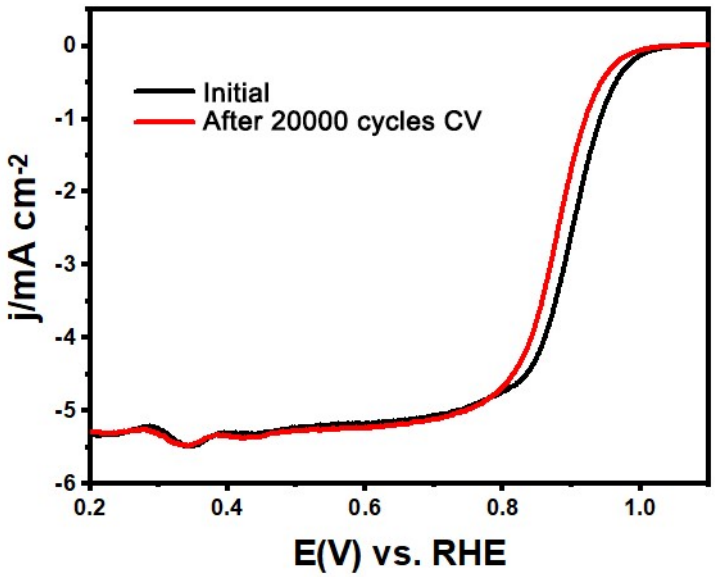

Figure S27. TEM image of the as-prepared Co_9S_8 $^{7.5}$NP/CA catalysts after the ADTs.

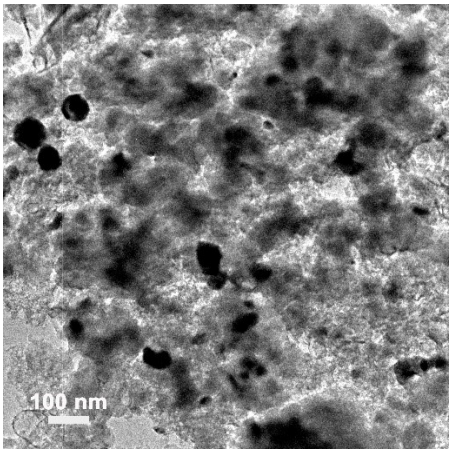

Figure S28. EIS spectra of (a) the as-prepared Co_9S_8 $^{7.5}$NP/CA catalysts and (b) pure Co_9S_8 NP/CA catalysts, measured at their separate overpotential.

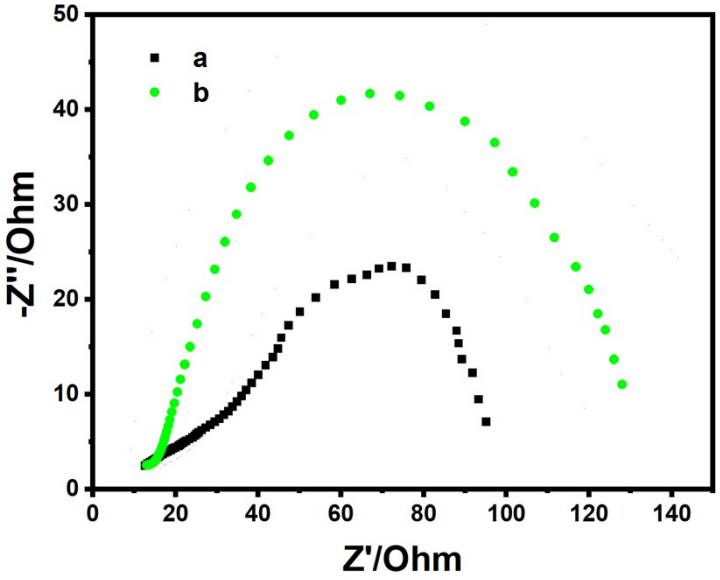

Figure S29. LSV curves of commercial Pt/C catalysts towards the acidic HER before and after the ADTs.

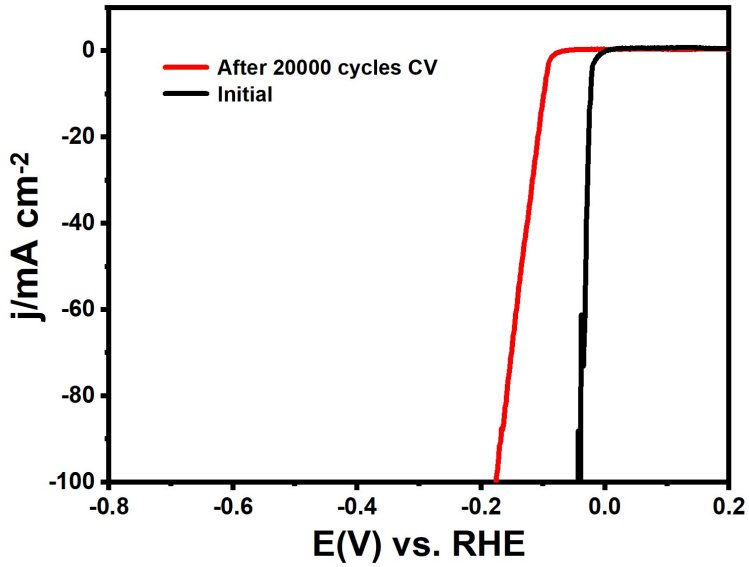

Table S1. The XPS fitting results of the as-prepared Co_9S_8 $^{7.5}$NP/CA catalysts and pure Co_9S_8 NP@CA catalysts.

Elements	Peaks						
C	C=C bond 284.6 eV		C-N bond 285.3 eV			C-O/C-S bond 286.7 eV	
N	pyridinic nitrogen 398.2 eV		pyrrolic nitrogen 399.3 eV		graphitic nitrogen 401.3 eV		oxidized nitrogen 403.9 eV
O	adsorbed oxygen 530.9 eV		C=O bond 531.9 eV			adsorbed water 533.1 eV	
S	$S\ 2p_{1/2}$ 165.1 eV		C-S-C species and $S\ 2p_{3/2}$ 163.9 eV			$C\text{-}SO_x\text{-}C$ species 168.8 eV	
Co			Co^{3+} state		Co^{2+} state		
	Co-S band		$Co\ 2p_{3/2}$	$Co\ 2p_{1/2}$	$Co\ 2p_{3/2}$	$Co\ 2p_{1/2}$	satellite peak
	778.4 eV	793.4 eV	781.3 eV	797.1 eV	783.6 eV	798.5 eV	803.1 eV

Table S2. The ORR and HER catalytic data of pure Co_9S_8 NP/CA catalysts, the as-prepared Co_9S_8 $^{7.5}$NP/CA catalysts, commercial Pt/C catalysts, Co_9S_8 ^{3}NP/CA catalysts, Co_9S_8 ^{5}NP/CA catalysts, Co_4S_3 ^{10}NP/CA catalysts and CA catalysts.

Samples	ORR			HER
	$E_{1/2}$ (V)	E_{onset} (V)	$\Delta E_{1/2\ (Pt)}$ (mV)	Overpotential (mV)
pure Co_9S_8 NP/CA catalysts	0.88	0.997	+15	239
Co_9S_8 $^{7.5}$NP/CA catalysts	0.891	1.050	+26	177
commercial Pt/C catalysts	0.865	1.030	0	24
Co_9S_8 ^{3}NP/CA catalysts	0.837	0.980	-28	269
Co_9S_8 ^{5}NP/CA catalysts	0.846	0.988	-19	182
Co_4S_3 ^{10}NP/CA catalysts	0.855	0.992	-10	233
CA catalysts	0.823	0.906	-42	534

Table S3. Chemical composition of each element and the corresponding atomic ratios (at%) of the as-prepared Co_9S_8 $^{7.5}$NP/CA catalysts and pure Co_9S_8 NP@CA catalysts obtained by XPS.

Samples	C (at. %)	N (at. %)	O (at. %)	S (at. %)	Co (at. %)
the as-prepared Co_9S_8 $^{7.5}$NP/CA catalysts	54.81	16.64	13.55	12.07	1.92
Pure Co_9S_8 @CA catalysts	64.66	14.26	13.85	6.61	0.62

Table S4. Comparison in the ORR performance between the as-prepared Co_9S_8 $^{7.5}$NP/CA catalysts and transition metal-based electrocatalysts reported in literatures.

Samples	$E_{1/2}$ (V vs. RHE)	E_{onset} (V vs. RHE)	Tafel slope (mV/dec)	Reference
the as-prepared Co_9S_8 $^{7.5}$NP/CA catalysts	0.891	1.050	58.0	**This work**
Fe-NCs	0.877	0. 963	46.0	[1]
(Fe, Co)SPPc-900-sp	0.830	0.936	62.0	[5]
Fe-NC/NG	0.830	0.910	78.7	[6]
NS-HPC	0.800	0.940	89.6	[7]
Fe/Ni–N–C	0.861	1.005	69.0	[8]
Ni-N4/GHSs/Fe-N4	0.830	0.930	81.0	[9]
La_2O_3-Co/AB	0.860	-	92.0	[10]

Table S5. Comparison in HER performance between the as-prepared Co_9S_8 $^{7.5}$NP/CA catalysts and transition metal-based electrocatalysts reported in the literature.

Samples	Overpotential (mV)	Tafel slope (mV/dec)	Reference
the as-prepared Co_9S_8 $^{7.5}$NP/CA catalysts	177	56	This work
Co-NCs	242	101	[1]
Co-BDC/MoS_2	248	86	[11]
N-doped Mo_2C nano particles	319	101.7	[12]
Ni-WSe_2	259	86	[13]
$MoSe_2$	267	77	[14]

References

1 Y. Wang, Y. Pan, L. Zhu, H. Yu, B. Duan, R. Wang, Z. Zhang and S. Qiu, *Carbon*, 2019, **146**, 671–679.

2 X. Liang, L. Wang, Y. Wang, J. Yun, Y. Sun and H. Xiang, *Materials Letters*, 2022, **307**, 131068.

3 D. Zhao, Z. Tang, W. Xu, Z. Wu, L.-J. Ma, Z. Cui, C. Yang and L. Li, *Journal of Colloid and Interface Science*, 2020, **560**, 186–197.

4 Z. Cao, M. Wu, H. Hu, G. Liang and C. Zhi, *NPG Asia Mater*, 2018, **10**, 670–684.

5 L. Chen, L. Cui, Z. Wang, X. He, W. Zhang and T. Asefa, *ACS Sustainable Chem. Eng.*, 2020, **8**, 13147–13158.

6 T. Wang, J. Feng, Q. Liu, X. Han and D. Wu, *Journal of Electroanalytical Chemistry*, 2022, **915**, 116326.

7 Y. Guo, T. Wang, D. Wu and Y. Tan, *Electrochimica Acta*, 2021, **366**, 137404.

8 H. Li, J. Wang, R. Qi, Y. Hu, J. Zhang, H. Zhao, J. Zhang and Y. Zhao, *Applied Catalysis B: Environmental*, 2021, **285**, 119778.

9 J. Chen, H. Li, C. Fan, Q. Meng, Y. Tang, X. Qiu, G. Fu and T. Ma, *Advanced Materials*, 2020, **32**, 2003134.

10 Q. Zhou, L. Zhang and X. Wang, *Applied Surface Science*, 2023, **610**, 155551.

11 D. Zhu, J. Liu, Y. Zhao, Y. Zheng and S. Qiao, *Small*, 2019, **15**, 1805511.

12 J. Jia, T. Xiong, L. Zhao, F. Wang, H. Liu, R. Hu, J. Zhou, W. Zhou and S. Chen, *ACS Nano*, 2017, **11**, 12509–12518.

13 S. R. Kadam, A. N. Enyashin, L. Houben, R. Bar-Ziv and M. Bar-Sadan, *J. Mater. Chem. A*, 2020, **8**, 1403–1416.

14 O. Zimron, T. Zilberman, S. R. Kadam, S. Ghosh, S. Kolatker, A. Neyman, R. Bar-Ziv and M. Bar-Sadan, *Isr. J. Chem.*, 2020, **60**, 624–629.